

SCIENTIFIC REPORTS



OPEN

A combined experimental and theoretical investigation on cellular blebbing

Chao Fang^{1,2}, T. H. Hui^{1,2}, X. Wei^{1,2}, X. Shao^{1,2} & Yuan Lin^{1,2}

Although accumulating evidence has demonstrated the important role of membrane blebbing in various cellular processes, the fundamental question of how the initiation/evolution of blebs are influenced by physical factors like membrane-cortex interactions and intracellular pressure remains unclear. Here, we report a combined modeling and experimental study to address this outstanding issue. Specifically, boundary integral method was used to track the motion of membrane (in 3D) during blebbing while possible rupture of the bilayer-cortex adhesion has also been taken into account. We showed that, for a given differential pressure across the cell membrane, the size of the weakened cortex must be over a critical value for blebbing to occur and the steady-state volume of a bleb is proportional to its initial growth rate, all in good agreement with recent experiments. The predicted shape evolution of blebs also matches well with our observations. Finally, a blebbing map, summarizing the essential physics involved, was obtained which exhibits three distinct regimes: no bleb formation corresponding to a low intracellular pressure or a small weakened cortex region; bleb formed with a fixed width when the disrupted cortex zone is very large; and a growing bleb resulted from progressive membrane-cortex detachment under intermediate weakened cortex size.

Cellular blebs are membrane protrusions caused by the detachment of the lipid bilayer from the underlying actin cortex. Besides serving as a hallmark for apoptosis, blebbing is also believed to play a role in various processes like cell spreading¹ and cytokinesis². For example, it has been suggested that blebs are critical for cells to maintain membrane tension homeostasis³. Recent evidence also indicated that migrating cells might have utilized blebbing in regulating their movement^{4–9}. For these reasons, intense research effort has been invested to understand how cell blebbing takes place as well as identify key factors governing this process. Specifically, it is well known now that the outgrowth of cell membrane (on regions with a weakened cortex) is driven by the intracellular hydrostatic pressure. The initially formed bleb can continue to grow, aided by the successive disruption of membrane-cortex adhesion, until a steady state size is reached^{4,10}. Interestingly, within a few minutes, the cortex can be re-formed underneath the bulged membrane which restores the actin contractility locally and eventually leads to the total retraction of the bleb¹¹. Theoretically, several attempts have also been made to describe the formation and evolution of cellular blebs. For instance, by assuming that the cross-membrane pressure difference is balanced by the passive tension in the lipid bilayer and the active cortical contraction collectively, a simple model was developed to predict the size of blebs as well as the threshold cortical tension for blebbing to take place¹². In addition, the formation of blebs has also been analyzed by treating the membrane as an elastic shell^{13–17}. Recently, following a different approach, the shape evolution of a cellular bleb was described by tracking the flow of cytosol^{18–21} as well as the transport and assembly of actins²².

It must be pointed out that many simplifications were made in these aforementioned investigations. For example, many studies focused on the static scenario only^{12,23} and the bleb is basically assumed to be spherical^{12,13,17,23}. In comparison, although the blebbing dynamics was considered in several models by tracking the flow of cytosol^{18–22}, the problem was examined in the two-dimensional configuration. Furthermore, despite that membrane-cortex connection was taken into account in previous studies on predicting the bleb shape^{14–16,20,21} or blebbing-assisted migration of cells¹⁹, the regulation of such interaction on the dynamics of blebbing (like how fast the bleb can grow and the critical pressure for blebbing to occur) has not been thoroughly examined. In reality, an initially formed bleb can continue to increase in size via successive rupture of bilayer-cortex adhesion

¹Department of Mechanical Engineering, The University of Hong Kong, Hong Kong SAR, China. ²HKU-Shenzhen Institute of Research and Innovation (HKU-SIRI), Shenzhen, Guangdong, China. Correspondence and requests for materials should be addressed to Y.L. (email: ylin@hku.hk)

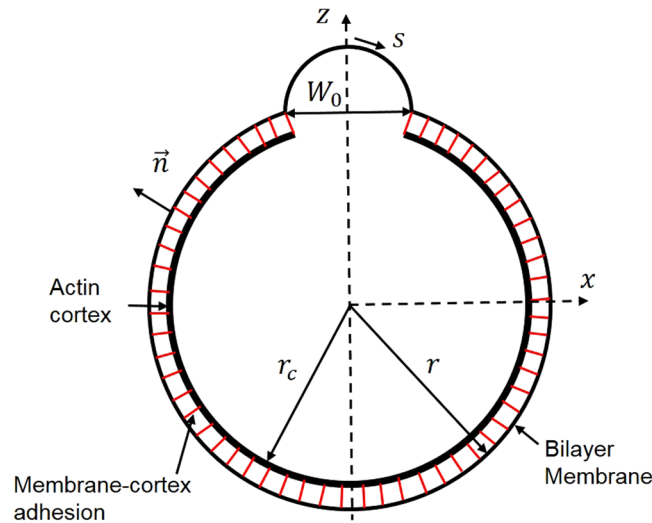


Figure 1. Schematic plot of a cellular bleb. The actin cortex is treated as rigid and stationary because of its high bending rigidity. r_c and r are the initial radii of the actin cortex and bilayer membrane, respectively. W_0 represents the size of the region where cortex is disrupted.

and assume a non-spherical shape because of transverse shear in the membrane and its cohesion with the cortex. Unfortunately, a theoretical 3D model capable of capturing these important features is still lacking. In addition, fundamental questions like how the formation and evolution of blebs are governed by key physical factors such as dynamic intracellular pressure level and initial cortex weakened size all remain unclear.

Here we report a combined modeling and experimental study to address these issues. Specifically, boundary integral method was used to track the motion of membrane (in 3D) during the blebbing process while possible rupture of the bilayer-cortex adhesion has also been considered. First of all, the predicted shape evolution of blebs from our model matches well with our experimental observations. Interestingly, it was also found that, for a given weakened size of the cortex, a threshold intracellular pressure is needed for bleb formation and the steady-state volume of a bleb is linearly proportional to its initial growth rate, all in well agreement with recent experiments^{12,24}. Finally, a blebbing map, summarizing the essential physics involved, was obtained which exhibits three distinct regimes: no bleb formation (corresponding to a very low intracellular pressure or a small weakened cortex region); bleb formed with a fixed width when the disrupted cortex is large, and a growing bleb resulted from progressive membrane-cortex detachment under intermediate weakened cortex size.

Theoretical Model for Cellular Blebbing

Consider the formation a membrane bleb over a region (with width W_0) where the cortex of a spherical suspension cell is disrupted, refer to Fig. 1. For simplicity, we proceed by assuming that the cytosol and culture fluid have the same viscosity (μ). As such, their movements can all be described by²⁵:

$$\mu \frac{\partial^2 u_i(\vec{y})}{\partial y_j^2} - \frac{\partial p(\vec{y})}{\partial y_i} + \vec{f}(\vec{y}) = 0 \quad (1a)$$

$$\frac{\partial u_i(\vec{y})}{\partial y_i} = 0 \quad (1b)$$

where μ represents the viscosity of cytosol (and the external fluid), \vec{y} refers to the position vector, u_i , p and \vec{f} are the fluid velocity along the i -th direction, pressure and the force density (arising from membrane elasticity and membrane-cortex adhesion) acting on the fluid by the membrane respectively. Note that the inertia effect has been neglected here given the over-damped nature of the system (i.e. the Stokes flow assumption). In addition, the flow field induced by blebbing is expected to vanish when moving far away from the cell, that is:

$$u_i = 0, \quad |\vec{y}| \rightarrow \infty \quad (2)$$

The cell membrane separating the cytosol and the medium can be treated as an immersed boundary, imposing the following conditions to the flow fields

$$[\vec{u}]_s = 0 \quad (3a)$$

$$[\sigma_{ij} n_i]_s = n_j \Delta \sigma \quad (3b)$$

where $[\cdot]_s$ stands for the jump of the function across the membrane (from the outside to the inside of cell), \vec{n} is the out-normal of the membrane surface S , σ_{ij} is the stress tensor within the fluid taking the form $\sigma_{ij} = -p\delta_{ij} + \left(\frac{\partial u_i}{\partial y_j} + \frac{\partial u_j}{\partial y_i} \right)$. Physically, equation (3a) means that the velocity field of the fluid must be continuous across the membrane, as well as satisfy the no-slip boundary condition there, while equation (3b) comes from the force equilibrium of the membrane. From the boundary integral approach, the velocity field can be expressed as²⁵

$$u_i(\vec{\xi}) = \iint_S u_i^j(\vec{\xi}, \vec{y}) n_j(\vec{y}) \Delta\sigma(\vec{y}) dS_{\vec{y}} \quad (4)$$

where

$$u_i^j(\vec{\xi}, \vec{y}) = -\frac{1}{8\pi\mu} \left(\frac{\delta_{ij}}{r} + \frac{(\xi_i - y_i)(\xi_j - y_j)}{r^3} \right), \quad r = |\vec{\xi} - \vec{y}| \quad (5)$$

is the so-called fundamental solution of the Stokes equation, located at point \vec{y} and oriented in the j -th direction. The term $\Delta\sigma$ appeared in equation (4) contains contributions from the bilayer membrane stretching σ_m , transverse membrane shear σ_s and membrane-cortex adhesion σ_a , i.e.

$$\Delta\sigma = \sigma_m + \sigma_s + \sigma_a \quad (6)$$

In this setup, all the components of $\Delta\sigma$ (i.e. σ_m , σ_s and σ_a) are assumed to be along the normal direction of the membrane. Furthermore, if the bilayer membrane is treated as linear elastic, then the tension γ_m inside can be related to the membrane area A as²⁶⁻²⁸

$$\gamma_m = K_A \frac{A - A_0}{A_0} \quad (7)$$

where K_A is the so-called area expansion modulus and A_0 is unstressed membrane area. Notice that, here the lipid membrane is basically assumed to have a uniform (equal-biaxial) tension everywhere, a treatment that is consistent with recent evidence that lipid flow takes place within milliseconds²⁹ and, hence, any blebbing-induced local stretch can quickly be distributed to the entire membrane. From Young-Laplace law, we have

$$\sigma_m = \gamma_m(C_1 + C_2) \quad (8)$$

where C_1 and C_2 stands for two principle curvatures of the curved membrane that can be expressed as $C_1 = -\frac{x'z'' - z'x''}{(x'^2 + z'^2)^{3/2}}$ and $C_2 = -\frac{z'}{x}$ ³⁰. Here, x' , z' , x'' , z'' are derivatives of s , where s is the arclength coordinate along the membrane (with $s=0$ corresponding to the zenith point of the cell), $x(s)$ is the distance from the symmetric axis at point s while $z(s)$ represents the vertical distance relative to the center of cortex (Fig. 1).

From the shell theory, σ_s can be calculated as³¹

$$\sigma_s = -\frac{1}{x} \frac{\partial(xq)}{\partial s} \quad (9)$$

where

$$q = \frac{1}{x} \frac{\partial x}{\partial s} \left[\frac{\partial(xm_1)}{\partial x} - m_2 \right] \quad (10)$$

is the transverse shear within membrane, $m_1 = K_b C_1$ and $m_2 = K_b C_2$ with K_b being the bending rigidity of membrane.

A linear cohesive law was used in the present study to describe membrane-cortex adhesion, that is σ_a is assumed to take the form

$$\sigma_a = \begin{cases} \sigma_c \cdot \frac{\delta}{\delta_c}, & 0 < \delta < \delta_c \\ 0, & \delta \geq \delta_c \end{cases} \quad (11)$$

where σ_c is the maximum traction (along the normal direction) the membrane-cortex adhesion can sustain while δ_c and δ are the critical and real separation between the bilayer membrane and actin cortex, respectively. Evidently, the quantity $\frac{1}{2}\sigma_c\delta_c$ represents the bilayer-cortex adhesion energy density which has been estimated to be of the order of $10^{-6.2} - 10^{-5} \text{ J/m}^2$ ³². Given that the cortex should be much stiffer than the lipid bilayer, its deformation is neglected here for simplicity (i.e. the cortex is assumed to be rigid).

With these descriptions at hand, the membrane velocities at time $t + \Delta t$ can be calculated from equation (4) based on its velocity field at the previous time step t . Specifically, to address the singularity issue in equation (5) (as \vec{y} approaches $\vec{\xi}$), we rewrite equation (4) as³³

$$u_i(\vec{\xi}) = \iint_S u_i^j(\vec{\xi}, \vec{y}) n_j(\vec{y}) [\Delta\sigma(\vec{y}) - \Delta\sigma(\vec{\xi})] dS_{\vec{y}} + \Delta\sigma(\vec{\xi}) \iint_S u_i^j(\vec{\xi}, \vec{y}) n_j(\vec{y}) dS_{\vec{y}} \quad (12)$$

Symbol	Physical meaning	Value	Ref
r	Initial radius of bilayer membrane	10 μm	Our experiment
r_c	Radius of actin cortex	9.9 μm	Estimated
W_0	Width of the initially weakened region	2.63 μm	Our experiment
μ	Cytosol dynamic viscosity	8 Pa · s	43
$\Delta\sigma$	Differential pressure	33.6 Pa	Our experiment
γ	Bilayer membrane tension	5 $\text{pN}/\mu\text{m}$	44,45
K_A	Areal expansion modulus	40 $\text{pN}/\mu\text{m}$	42
K_b	Bending rigidity	10–20 $k_b T$	35
σ_c	Maximum adhesion traction	125 Pa	32
δ_c	Critical membrane-cortex separation	0.04 μm	46

Table 1. Parameters list of boundary integral model.

Note that, the first term on the right hand side of equation (12) is a regular integral now while the second term vanishes for any closed shape of membrane (see³³ for details). Therefore, we have

$$u_i(\vec{\xi}) = \iint_S u_j^i(\vec{\xi}, \vec{y}) n_j(\vec{y}) [\Delta\sigma(\vec{y}) - \Delta\sigma(\vec{\xi})] dS_{\vec{y}} \quad (13)$$

Results

Based on our experimental observations, the width W_0 of the initially weakened cortex region was chosen to be 2.63 μm . The values of other parameters (unless stated otherwise) are listed in Table 1.

Our simulation showed that the bilayer membrane bulges first on the weakened part and then forms a bleb whose size continues to grow (aided by progressive membrane-cortex detachment) before a steady state is reached, refer to Fig. 2. In comparison, the shape and size evolution of blebs observed in our experiment are also shown in Fig. 2. Clearly, we can see that good agreement between simulation and experiment has been achieved.

It is well known that the growth of bleb is driven by the unbalanced differential pressure ($\Delta\sigma$), between inside and outside of the cell, pushing the cytosol into the bleb. Initially, such unbalanced pressure is maximum because of the sudden removal of the cortex (and hence the membrane-cortex adhesion σ_a , see equation (6)). As the bleb grows, the intracellular pressure gradient drops due to the viscous flow of the cytosol. At the same time, the principal curvatures (C_1 and C_2) of the blebbed region, along with the overall membrane area (A), increase leading to elevated membrane forces σ_m and σ_s on the right side of equation (6). Eventually, $\Delta\sigma$ (referred to as the pressure in the cell body in Fig. 3) will be completely offset by bleb membrane forces $\sigma_m + \sigma_s$ when the steady-state is reached (Fig. 3).

Bleb formation regulated by intracellular pressure and membrane-cortex adhesion. Previous studies have shown that the magnitude of differential pressure ($\Delta\sigma$) plays a key role in bleb formation¹². Specifically, for a spherical cell with radius r , this pressure will be balanced by the total membrane tension T through the Young-Laplace law as $\Delta\sigma = 2T/r$ with $T = \gamma_c + \gamma$ where γ represents the tension in the lipid bi-layer while γ_c stands for cortical tension originated from actomyosin contraction. However, γ_c vanishes in the region where cortex is disrupted, which eventually leads to the outgrowth of the bi-layer. By assuming the bleb possesses a spherical geometry, Tinevez and co-workers estimated the critical value of $\Delta\sigma$ for bleb formation to be $\Delta\sigma \sim 4\gamma/W_0$, with W_0 being the size of the weakened region of cortex¹². That is, no apparent bleb will be formed if the differential pressure is below this threshold level. Interestingly, similar trend was also revealed by our simulations. In particular, as shown in Fig. 4a, the steady-state bleb volume became significant only when the intracellular pressure is above a critical level. Furthermore, not surprisingly, the value of this threshold pressure increases with the bi-layer tension, i.e. when the percentage of cortical contraction in the overall membrane tension decreases. Specifically, when $\gamma = 15 \text{ pN}/\mu\text{m}$ and $W_0 = 2.63 \mu\text{m}$, the critical $\Delta\sigma$ was found to be around 22.08 Pa from our simulations [Fig. 4a], in good agreement with the value ($\sim 20 \text{ Pa}$) estimated by Tinevez *et al.*¹². The small difference may come from fact that possible failure of membrane-cortex adhesion (i.e. the breaking of membrane-cortex “links” as schematically shown in Fig. 1) was taken into account in our formulation. That is, W_0 can grow in our simulations while this quantity was fixed in the simple estimation model¹². In this regard, it is conceivable that the critical $\Delta\sigma$ for bleb formation is also regulated by the strength (σ_c) of membrane-cortex cohesion. Indeed, as illustrated in Fig. 4b, a higher pressure level must be reached to trigger blebbing as σ_c increases.

Another interesting observation from previous investigations is that the final bleb volume seems to be proportional to its initial growth rate²⁴. To see whether similar conclusion can be obtained from our model, we tracked the volume evolution of blebs formed under different intracellular pressure. Obviously, the bleb grows faster as $\Delta\sigma$ increases as shown in Fig. 5a. By plotting the volume growth rate within the first 0.2 s against the steady-state bleb volume, a linear relationship was indeed observed [Fig. 5b].

To further test the model, we have compared our simulations to another set of experiments³² where the perimeter and neck radius of a growing bleb in M2 cell as functions of time were carefully measured (refer to the square and diamond symbols in Fig. 6). In comparison, these quantities predicted from our model are also shown in

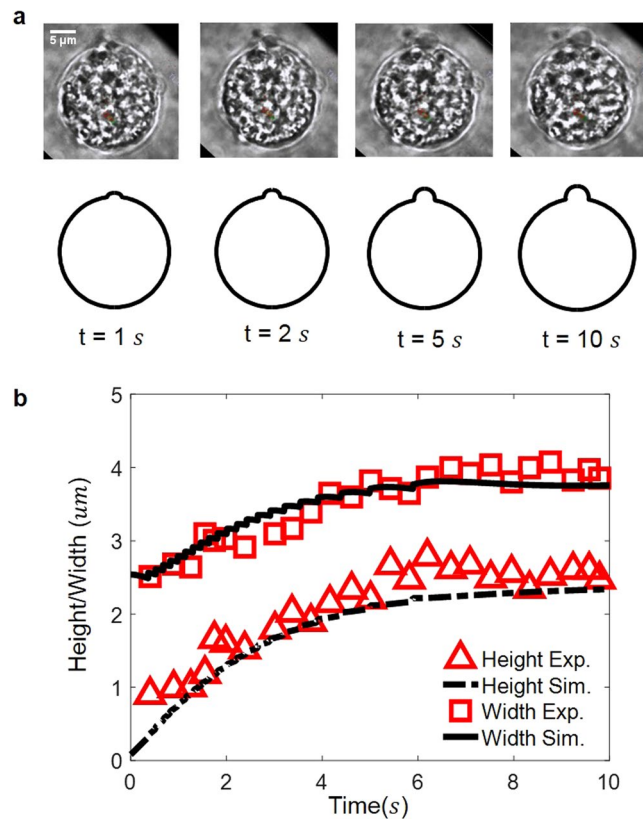


Figure 2. (a) Comparison between the observed bleb profile (top panel), captured by phase contrast microscopy in our experiment, and the predicted bleb shapes (bottom panel). (b) Evolution of the bleb height and width where simulation and experimental results are represented by lines and symbols, respectively. Sudden jumps in the simulation curve come from the failure of individual cohesive element.

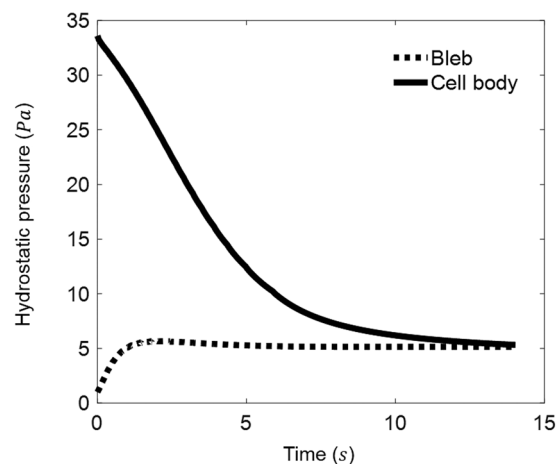


Figure 3. Evolution of the cell body pressure ($\Delta\sigma$) and the bleb pressure (defined as $\sigma_m + \sigma_s$ in equation (6)) during the blebbing process.

Fig. 6 by solid lines. Evidently, excellent agreement between theory and experiment has been achieved. It must be pointed out that the membrane tension, initial weakened size and adhesion energy were chosen as $\gamma = 2pN/um$, $W_0 = 1.5 um$, and $\Gamma = 5 \times 10^{-6} J/m^2$ in this simulation, respectively, which are all well within the range reported/estimated³² (i.e. $\gamma \sim 0.8-6pN/um$, $W_0 \sim 1.3-1.6 um$, $\Gamma \sim 1.3-9.8 \times 10^{-6} J/m^2$). In addition, the fact that the observed neck radius (of the bleb) kept increasing indicates that gradual detachment between the lipid membrane and cortex indeed took place during the blebbing process, a feature that has been captured by the present model.

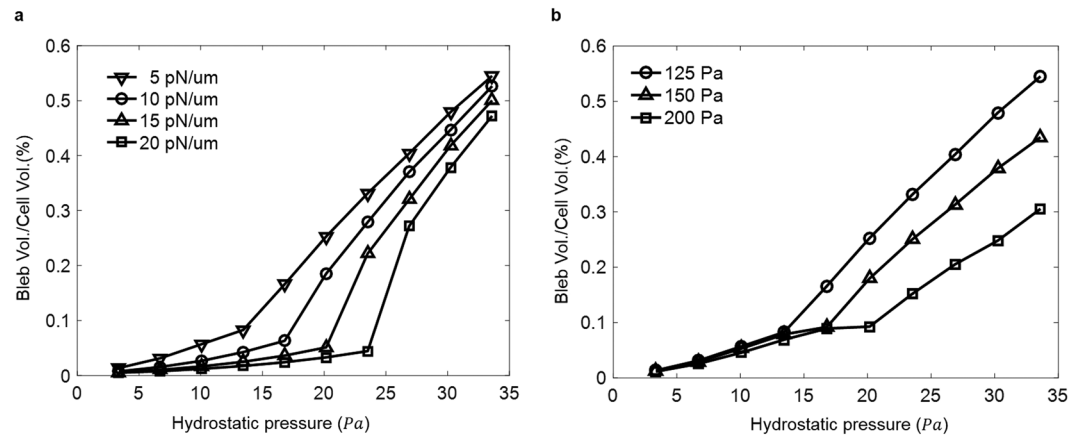


Figure 4. The critical differential pressure for bleb formation is influenced by both the bilayer membrane tension (a) and membrane-cortex adhesion strength (b). When $\Delta\sigma$ is beyond a threshold value, membrane-cortex adhesion begins to fail and propagates, resulting in a significant growth in the steady-state bleb volume (normalized by the initial cell volume).

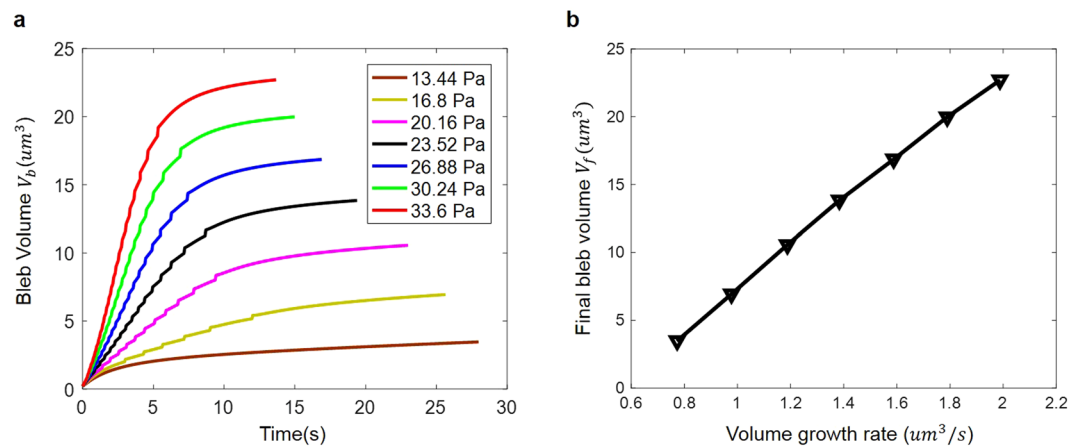


Figure 5. (a) The bleb volume (V_b) as a function of time under different differential pressure $\Delta\sigma$. (b) Steady-state bleb volume (V_f) is proportional to its initial growth rate, i.e. $V_f \sim dV_b/dt$ as $t \rightarrow 0$.

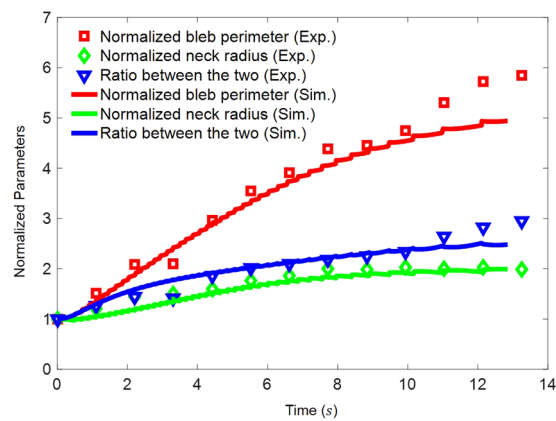


Figure 6. Evolution of the bleb perimeter (i.e. arc-length in 2D) and neck radius. Experiment data shown here are extracted from the work by Charras *et al.*³².

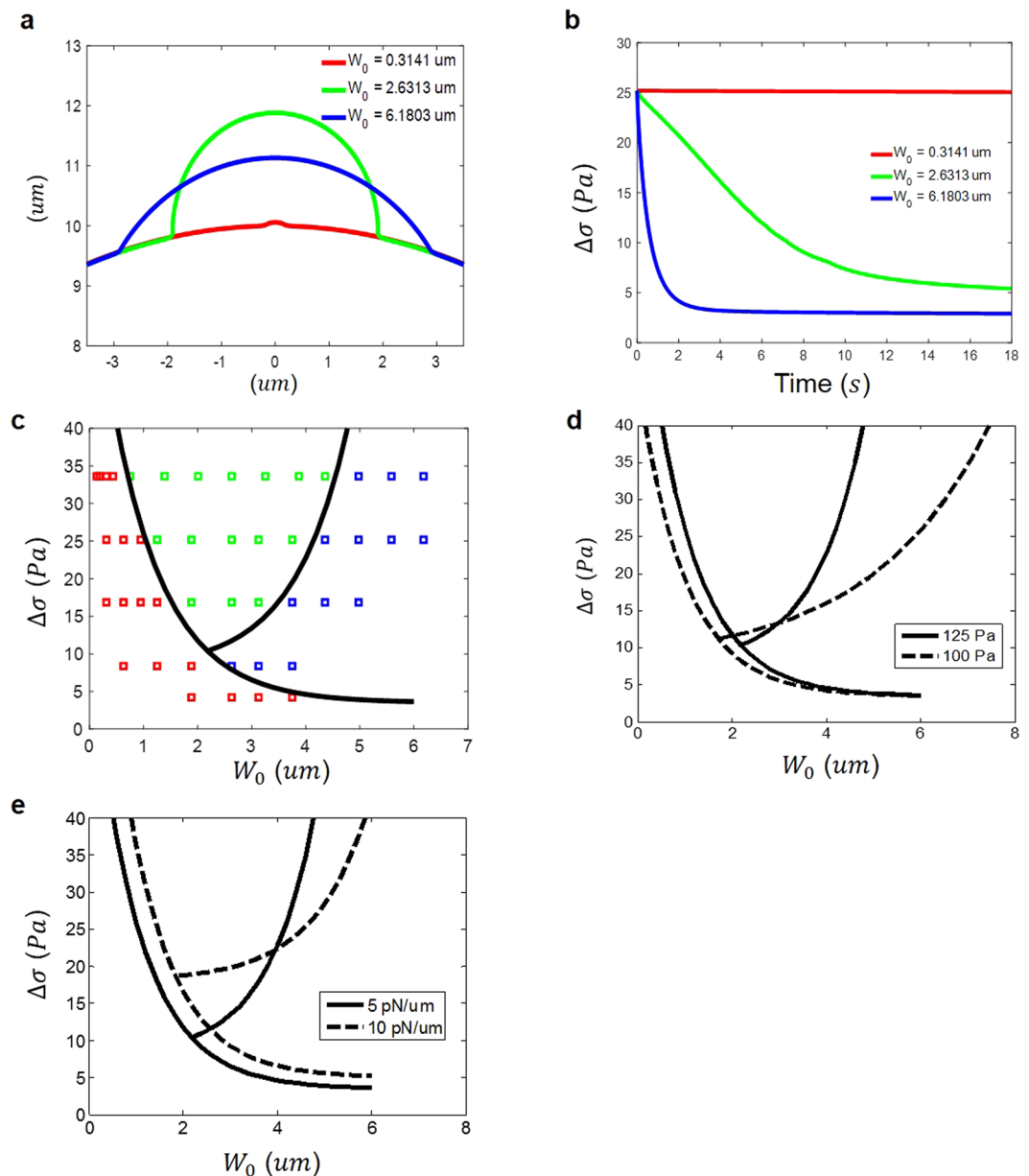


Figure 7. (a) Final profile of the bleb under different initial weakened size of cortex W_0 . (b) Temporal evolution of the differential pressure under different values of W_0 . (c) Three different scenarios: no apparent blebbing (red), bleb formation with a growing (green) or fixed (blue) width. Varying the membrane-cortex adhesion strength (d) or bilayer tension (e) will shift the boundaries of these three regions slightly without altering the main features.

Blebbing map. Besides differential pressure and cortex-membrane cohesion, it is natural to believe that the initial size of the weakened cortex also plays a key role in the formation of blebs. For example, by considering the pressure-driven peeling of membrane from the cortex, Alert and Casademunt found that a bleb can only be nucleated from a weakened region with size over 100–200 nm³⁴. However, the influence of cytosol flow was neglected there. Here, a parametric study on the blebbing process is conducted to unambiguously address this issue. Specifically, the steady-state shapes of the deformed membrane under different weakened size W_0 are shown in Fig. 7a.

Clearly, when W_0 is small, the bilayer membrane can only bulge slightly, that is without apparent bleb formation [Fig. 7a]. In comparison, as the weakened size increases a bleb will form and actually keep growing (by inducing successive membrane-cortex separation) before reaching a steady state size. Interestingly, when W_0 becomes relatively large no rupture of membrane-cortex adhesion will be triggered and the bleb will be developed with a fixed width. To understand these intriguing findings, we examined the temporal evolution of the differential pressure $\Delta\sigma(t)$ during the blebbing process. As shown in Fig. 7b, negligible change in this quantity took place under small W_0 , reflecting the fact that very little membrane bulging and hence fluid movement were resulted in

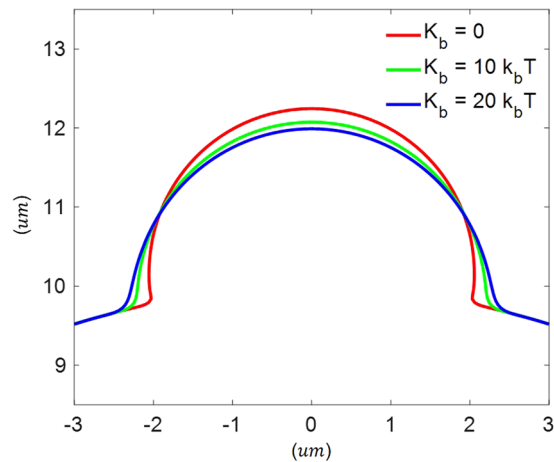


Figure 8. Steady-state shape of blebs under different membrane bending rigidities.

this case. On the other hand, under intermediate weakened size, a gradual decrease in $\Delta\sigma$ was observed indicating significant cytosol flow has been triggered to sustain the growth of the bleb. However, a sharp drop in the differential pressure occurred when W_0 is large, presumably because a huge volume of cytosol has flowed into the bleb. Such big drop in $\Delta\sigma$ was likely to be the reason for no additional rupture of membrane-cortex adhesion during the blebbing process. These results are best summarized in the so-called blebbing map as shown in Fig. 7c. Essentially, when the initial differential pressure is low, the system will transit from no apparent blebbing to the formation of bleb with a fixed width as W_0 increases. However, under relatively large initial value of $\Delta\sigma$, the scenario of a bleb formed with an increasing width appears at intermediate W_0 . Changing the strength of membrane-cortex adhesion or the bi-layer tension level will only shift the boundaries of these three regions slightly [Fig. 7d and e], but maintain these main features mentioned above.

Effect of membrane bending rigidity. The present model also allows us to examine how cellular blebbing is influenced by the bending rigidity of the bilayer membrane, although its value is commonly believed to be in the range of 10–20 $k_b T^{35}$ with $k_b T$ being the thermal energy. As illustrated in Fig. 8, a sharp angle between the bilayer and the un-blebbed part of membrane (i.e. with cortex support underneath) was formed at the edge of the bleb when the bending of the bilayer is neglected. However, a much smoother transition was observed once a non-vanishing bending rigidity is used. Energetically, this is not surprising because a sharp angle corresponds to large membrane curvatures locally, eventually leading to an exceedingly high bending energy stored inside. These results also indicate that factors like bilayer tension and membrane-cortex adhesion should play a more significant role, compared to membrane bending, in determining the steady-state bleb size.

Discussion

In conclusion, we have presented a combined modeling and experimental study on the phenomenon of cell blebbing here. By taking into account possible rupture of the bilayer-cortex adhesion and the 3D nature of a cellular bleb, the roles of different physical factors such as intracellular pressure, the size of the weakened cortex and bending rigidity of bilayer membrane in the blebbing process have all been elucidated. Specifically, we presented that, for a given weakened size of the cortex, a threshold differential pressure across the membrane is needed for bleb formation and the steady-state volume of a bleb is linearly proportional to its initial growth rate, all in well agreement with experiments^{12,24}. Moreover, a blebbing map, summarizing the essential physics involved, was obtained which shows that there three distinct scenarios: no bleb formation (corresponding to a very low intracellular pressure or a small weakened cortex region); bleb formed with a fixed width when the disrupted cortex is large, and a growing bleb resulted from progressive membrane-cortex detachment under intermediate weakened cortex size. Varying the strength of membrane-cortex adhesion and/or bilayer tension will shift the boundaries of these three regions, making it easier (or harder) for a bleb to be nucleated/formed which again is in broad agreement with recent experimental observations³². It must be pointed out that a regime of uncontrollable bleb growth was predicted in some previous studies^{12,21} when the membrane stiffness is relative low (or, equivalently, when the intracellular pressure is very high). However, no such phenomenon was observed in our simulations even when K_A was varied from 40 to 1 pN/ μm . We believe the main reason is that, unlike in ref.²¹, gradual detachment between the cortex and bilayer membrane was allowed in our model, which effectively serves a dissipation mechanism to absorb the unbalanced intracellular pressure during the blebbing process. As a result, the cell body pressure dropped rapidly in our simulations (refer to Fig. 3), eventually leading to blebs with a steady-state size. Interestingly, it seems that similar finding has also been obtained in the study by Lim and co-workers¹⁹, where (like the present study) cortex-membrane adhesion/rupture was taken into account and no uncontrollable bleb growth was reported.

Given the important role of membrane blebbing in various cellular processes, this work may help us understand how cells execute their biological duties. For example, evidences have suggested that processes like turnover

of cell-extracellular matrix adhesions, cortex remodeling and blebbing are tightly coordinated during the locomotion of cells^{6–9}. In addition, it is also believed that, as part of the membrane recycling system, cell blebbing works with endocytosis and exocytosis for cells to achieve homeostasis (in terms of membrane tension or the intracellular pressure). Interestingly, cortex rearrangement often takes place over minutes^{36,37} while the frequency of exocytosis in a non-migrating cell is usually less than one per minute³⁸, indicating that these factors may not be very important in the rapid blebbing process (taking ~10–20 seconds to complete). However, they can certainly play a role in related phenomena like the nucleation/retraction of blebs³⁹, cell motility and homeostasis regulation of cells. It is conceivable that our model can serve as a platform to systematically examine these issues. Finally, the blebbing map obtained here could be useful in the design of (and be tested by) future experiments. In particular, it will be interesting to see, by varying quantities like membrane tension and the strength of cortex-membrane adhesion experimentally, whether the occurrence and transition of different blebbing modes predicted here can indeed be observed. Such information will undoubtedly enhance our understanding of this intriguing phenomenon. Indeed, investigations along these lines are underway.

Materials and Methods

Cell culture. K562 cells, derived from a chronic myeloid leukemia patient with blast crisis^{40,41} were cultured in DMEM medium (Gibco) containing 10% fetal bovine serum (Invitrogen). To mimic the native biological environment *in vivo*, the experiment was conducted with the presence of 5% CO₂ supply (Warner Instruments) and the temperature was controlled by a temperature regulator (Warner Instruments) at 37 degree Celsius.

Blebbing induction and analysis. To induce cortical-weakened bleb formation⁸, K562 cells were exposed to cytochalasin D which is known to disrupt the actin cytoskeleton and hence promote bleb nucleation^{11,32}. Specifically, 5 μ M of cytochalasin D was added to the culture medium of K562 cells for 5 minutes. Once a cellular bleb started to nucleate, its shape evolution was closely monitored by an optical microscopy with 1000X magnification (Nikon) from which the bleb height and width were estimated by the software ImageJ.

Membrane tension/Differential pressure measurement. Micropipette aspiration was used to measure the overall membrane tension (or equivalent the initial differential pressure) of cells⁴². Specifically, the tips of glass micropipettes, prepared by micropipette pullers (Sutter Instrument), were polished with a microforge (Nikon) to achieve a desired inner radius (R_p). The micropipette was then mounted on a motorized stage and connected to a syringe providing suction pressures. An alcoholic multi-tube manometer (tequipment) was used to record the negative pressure produced by the syringe. During the test, the pipette was first loaded at the same depth of the targeted cell and then moved horizontally to approach it. The suction pressure was applied when an initial tip-cell separation of 30 μ m was reached. Once the cell was grabbed by the micropipette, we gradually increased the suction pressure until it reaches a critical value P_c , beyond which the whole cell will be sucked into the pipette spontaneously. Under this critical pressure, the portion of the cell being sucked into the pipette will approximately form a hemisphere (with radius R_p) while the portion remained outside assumes a radius R_c . The overall membrane tension γ_0 (i.e. the summation of cortical and bi-layer tensions) can then be related to P_c , R_p and R_c as⁴²

$$\gamma_0 = \frac{P_c}{2} \left(\frac{1}{R_p} - \frac{1}{R_c} \right)^{-1} \quad (14)$$

After that, the initial differential pressure $\Delta\sigma$ was calculated from γ_0 and the cell radius via the Laplace law.

Numerical scheme. To evaluate the membrane movement from the integral equation (13), a numerical scheme was developed using MATLAB. Specifically, the entire (axisymmetric) membrane was meshed along the meridional and equatorial directions with 130 and 60 elements, respectively. The elements are quadratic with 3×3 nodes each. After that, the blebbing process is simulated by repeating the following steps

- (1) Calculate the principal curvatures, as well as the bending moments m_1 and m_2 , in each element by assuming quadratic dependence of variables on both x and z ;
- (2) Compute each components of $\Delta\sigma$ from equations (7–11);
- (3) Average/smooth the values of $\Delta\sigma$ calculated from different neighboring elements and then evaluate the membrane velocity from equation (13) by Gaussian quadrature integration (see ref.³¹ for more details);
- (4) Employ the forward Euler method to track the movement of the bilayer membrane.

It must be pointed out that severe element distortion may occur near the bleb neck. Therefore, constant re-meshing was carried out to eliminate possible errors/instability induced by this. In addition, simulations with different element sizes have also been conducted to make sure that results presented here are mesh-size independent³³.

References

1. Norman, L. L., Sengupta, K. & Aranda-Espinoza, H. Blebbing dynamics during endothelial cell spreading. *Eur. J. Cell Biol.* **90**, 37–48 (2011).
2. Tokumitsu, T. & Maramorosch, K. Cytoplasmic protrusions in insect cells during mitosis *in vitro*. *J. Cell Biol.* **34**, 677–683 (1967).
3. Norman, L. L., Brugués, J., Sengupta, K., Sens, P. & Aranda-Espinoza, H. Cell blebbing and membrane area homeostasis in spreading and retracting cells. *Biophys. J.* **99**, 1726–1733 (2010).

4. Charras, G. & Paluch, E. Blebs lead the way: how to migrate without lamellipodia. *Nat. Rev. Mol. Cell Biol.* **9**, 730–736 (2008).
5. Lorentzen, A., Bamber, J., Sadok, A., Elson-Schwab, I. & Marshall, C. J. An ezrin-rich, rigid uropod-like structure directs movement of amoeboid blebbing cells. *J. Cell Sci.* **124**, 1256–1267 (2011).
6. Bergert, M., Chandradoss, S. D., Desai, R. A. & Paluch, E. Cell mechanics control rapid transitions between blebs and lamellipodia during migration. *Proc. Natl. Acad. Sci. USA* **109**, 14434–14439 (2012).
7. Fackler, O. T. & Grosse, R. Cell motility through plasma membrane blebbing. *J. Cell Biol.* **181**, 879–884 (2008).
8. Paluch, E. K. & Raz, E. The role and regulation of blebs in cell migration. *Curr. Opin. Cell Biol.* **25**, 582–590 (2013).
9. Maugis, B. *et al.* Dynamic instability of the intracellular pressure drives bleb-based motility. *J. Cell Sci.* **123**, 3884–3892 (2010).
10. Charras, G. T. A short history of blebbing. *J. Microsc.* **231**, 466–478 (2008).
11. Charras, G. T., Hu, C. K., Coughlin, M. & Mitchison, T. J. Reassembly of contractile actin cortex in cell blebs. *J. Cell Biol.* **175**, 477–490 (2006).
12. Tinevez, J. Y. *et al.* Role of cortical tension in bleb growth. *Proc. Natl. Acad. Sci. USA* **106**, 18581–18586 (2009).
13. Woolley, T. E. *et al.* Three mechanical models for blebbing and multi-blebbing. *IMA J. Appl. Math.* **79**, 636–660 (2014).
14. Woolley, T. E. *et al.* Cellular blebs: pressure-driven, axisymmetric, membrane protrusions. *Biomech. Model. Mechanobiol.* **13**, 463–476 (2014).
15. Woolley, T. E. *et al.* Global contraction or local growth, bleb shape depends on more than just cell structure. *J. Theor. Biol.* **380**, 83–97 (2015).
16. Woolley, T. E., Gaffney, E. A. & Goriely, A. Membrane shrinkage and cortex remodelling are predicted to work in harmony to retract blebs. *R. Soc. Open Sci.* **2**, 150184 (2015).
17. Woolley, T. E., Gaffney, E. A. & Goriely, A. Random blebbing motion: A simple model linking cell structural properties to migration characteristics. *Phys. Rev. E* **96**, 012409 (2017).
18. Lim, F. Y., Chiam, K. H. & Mahadevan, L. The size, shape, and dynamics of cellular blebs. *EPL* **100**, 28004 (2012).
19. Lim, F. Y., Koon, Y. L. & Chiam, K.-H. A computational model of amoeboid cell migration. *Comput. Methods. Biomech. Biomed. Eng.* **16**, 1085–1095 (2013).
20. Strychalski, W. & Guy, R. D. A computational model of bleb formation. *Math. Med. Biol.* **30**, 115–130 (2012).
21. Strychalski, W. & Guy, R. D. Intracellular pressure dynamics in blebbing cells. *Biophys. J.* **110**, 1168–1179 (2016).
22. Young, J. & Mitran, S. A numerical model of cellular blebbing: a volume-conserving, fluid-structure interaction model of the entire cell. *J. Biomech.* **43**, 210–220 (2010).
23. Hu, J. *Mathematical Modeling and Analysis of in vitro Actin Filament Dynamics and Cell Blebbing*. Ph.D thesis, University of Minnesota (2009).
24. Cunningham, C. C. Actin polymerization and intracellular solvent flow in cell surface blebbing. *J. Cell Biol.* **129**, 1589–1599 (1995).
25. Power, H. & Wrobel, L. C. *Boundary Integral Methods in Fluid Mechanics*. (Computational Mechanics Publications, 1995).
26. Secomb, T. W. Interaction between bending and tension forces in bilayer membranes. *Biophys. J.* **54**, 743–746 (1988).
27. Fisher, J. L. & Margulies, S. S. Modeling the effect of stretch and plasma membrane tension on Na⁺-K⁺-ATPase activity in alveolar epithelial cells. *Am. J. Physiol. Lung Cell Mol. Physiol.* **292**, L40–L53 (2007).
28. Diz-Muñoz, A., Fletcher, D. A. & Weiner, O. D. Use the force: membrane tension as an organizer of cell shape and motility. *Trends Cell Biol.* **23**, 47–53 (2013).
29. Keren, K. *et al.* Mechanism of shape determination in motile cells. *Nature* **453**, 475–480 (2008).
30. Yi, X. & Gao, H. Cell membrane wrapping of a spherical thin elastic shell. *Soft Matter* **11**, 1107–1115 (2015).
31. Pozrikidis, C. Effect of membrane bending stiffness on the deformation of capsules in simple shear flow. *J. Fluid Mech.* **440**, 269–291 (2001).
32. Charras, G. T., Coughlin, M., Mitchison, T. J. & Mahadevan, L. Life and times of a cellular bleb. *Biophys. J.* **94**, 1836–1853 (2008).
33. Pozrikidis, C. *Boundary Integral and Singularity Methods for Linearized Viscous Flow*. (Cambridge University Press, 1992).
34. Alert, R. & Casademunt, J. Bleb nucleation through membrane peeling. *Phys. Rev. Lett.* **116**, 068101 (2016).
35. Boal, D. *Mechanics of the Cell*. (Cambridge University Press, 2012).
36. Lappalainen, P. & Drubin, D. G. Cofilin promotes rapid actin filament turnover *in vivo*. *Nature* **388**, 78 (1997).
37. Mallavarapu, A. & Mitchison, T. Regulated actin cytoskeleton assembly at filopodium tips controls their extension and retraction. *J. Cell Biol.* **146**, 1097–1106 (1999).
38. Gauthier, N. C., Fardin, M. A., Roca-Cusachs, P. & Sheetz, M. P. Temporary increase in plasma membrane tension coordinates the activation of exocytosis and contraction during cell spreading. *Proc. Natl. Acad. Sci. USA* **108**, 14467–14472 (2011).
39. Collier, S., Paschke, P., Kay, R. R. & Bretschneider, T. Image based modeling of bleb site selection. *Sci. Rep.* **7**, 6692 (2017).
40. Koeffler, H. & Golde, D. Human myeloid leukemia cell lines: a review. *Blood* **56**, 344–350 (1980).
41. Sawyers, C. L. Chronic myeloid leukemia. *N. Engl. J. Med.* **340**, 1330–1340 (1999).
42. Hochmuth, R. M. Micropipette aspiration of living cells. *J. Biomech. Eng.* **33**, 15–22 (2000).
43. Wirtz, D. Particle-tracking microrheology of living cells: principles and applications. *Annu. Rev. Biophys.* **38**, 301–326 (2009).
44. Dai, J. & Sheetz, M. P. Membrane tether formation from blebbing cells. *Biophys. J.* **77**, 3363–3370 (1999).
45. Simson, R. *et al.* Membrane bending modulus and adhesion energy of wild-type and mutant cells of *Dictyostelium* lacking talin or cortaxillins. *Biophys. J.* **74**, 514–522 (1998).
46. Liu, D. *et al.* Single-molecule detection of phosphorylation-induced plasticity changes during ezrin activation. *FEBS Lett.* **581**, 3563–3571 (2007).

Acknowledgements

This work was supported by grants from the Research Grants Council (Project Nos. HKU 17205114, HKU 17211215, HKU 17257016) of the Hong Kong Special Administration Region and the National Natural Science Foundation of China (Project No. 11572273).

Author Contributions

Y.L. conceived the study. C.F. and X.W. carried out the modeling and simulation. T.H.H. and X.S. performed experiments and analyzed data. C.F., T.H.H. and Y.L. wrote the manuscript. All authors reviewed the manuscript.

Additional Information

Competing Interests: The authors declare that they have no competing interests.

Publisher's note: Springer Nature remains neutral with regard to jurisdictional claims in published maps and institutional affiliations.



Open Access This article is licensed under a Creative Commons Attribution 4.0 International License, which permits use, sharing, adaptation, distribution and reproduction in any medium or format, as long as you give appropriate credit to the original author(s) and the source, provide a link to the Creative Commons license, and indicate if changes were made. The images or other third party material in this article are included in the article's Creative Commons license, unless indicated otherwise in a credit line to the material. If material is not included in the article's Creative Commons license and your intended use is not permitted by statutory regulation or exceeds the permitted use, you will need to obtain permission directly from the copyright holder. To view a copy of this license, visit <http://creativecommons.org/licenses/by/4.0/>.

© The Author(s) 2017